nature portfolio

https://doi.org/10.1038/s41563-021-00993-6

Supplementary information

Fast crystal growth at ultra-low temperatures

In the format provided by the authors and unedited

Supplementary Information for

"Fast crystal growth at ultra-low temperatures"

Qiong Gao[1,9], Jingdong Ai[2,9], Shixiang Tang[1], Minhuan Li[1],
Yanshuang Chen[1], Jiping Huang[1], Hua Tong[3,4,5], Lei Xu [6]
Limei Xu[2,7] *, Hajime Tanaka[3,8†] & Peng Tan[1] ‡

[1] *State Key Laboratory of Surface Physics and Department of Physics, Fudan University, Shanghai 200433, China*

[2] *International Centre for Quantum Materials and School of Physics, Peking University, Beijing 100871, China*

[3] *Department of Fundamental Engineering, Institute of Industrial Science, University of Tokyo, 4-6-1 Komaba, Meguro-ku, Tokyo 153-8505, Japan*

[4] *School of Physics and Astronomy, Shanghai Jiao Tong University, 800 Dong Chuan Road, Shanghai, 200240, China*

[5] *Department of Physics, University of Science and Technology of China, Hefei 230026, China*

[6] *Department of Physics, The Chinese University of Hong Kong, Hong Kong, China*

[7] *Collaborative Innovation Center of Quantum Matter, Beijing, China*

[8] *Research Center for Advanced Science and Technology, University of Tokyo, 4-6-1 Komaba, Meguro-ku, Tokyo 153-8505, Japan*

[9] *These authors contributed equally: Qiong Gao, Jingdong Ai*

* limei.xu@pku.edu.cn
† tanaka@iis.u-tokyo.ac.jp
‡ tanpeng@fudan.edu.cn

Supplementary Discussion

Role of the crystal-liquid density difference in glass mechanical stability

Next, we focus on the additional effects of the nature of interparticle interactions. We find a considerable difference in the density variation across the interface accompanied by the structural ordering between soft long-range-interaction and hard short-range-interaction systems. In the low-ϕ charged colloidal systems, the density change across the interface (less than 1 %) is smaller than the density fluctuation amplitude in the liquid, and this feature is nearly T-independent (see Fig. S5, Fig. S6a and Figs. S7-S11 in Supplementary Information). In contrast, for a high-ϕ sample with hard short-range interaction, the density change across the crystal-glass interface (nearly 20 %) is much larger than the density fluctuation amplitude in the amorphous region (see Figs. S6b and S12). These observations suggest that the glass's mechanical stability increases with an increase in the crystal-liquid density mismatch. Note that the more considerable density increase upon crystallization means a weaker driving force of crystallization. Therefore, the harder the interaction is, the larger the crystal-liquid density mismatch is and the more rigid the icosahedral structures are, making the glass state more stable against diffusionless fast crystal growth.

Furthermore, our analyses show no apparent density decrease near the interface in both soft-sphere systems where crystals keep growing and hard-sphere-like glass systems where crystals stop growing. Thus, the interface mobility enhancement is primarily caused by the disordered state's mechanical instability and not by the density reduction. Such instability more easily occurs by (1) increasing the interaction softness or (2) decreasing the packing fraction.

The latter mechanism (2) should also work for hard-sphere systems, which might explain the crystallization of only the top half part of a hard-sphere glass reported in Refs. [1–3]. First, surface-induced preordering at the sample's air-liquid interface or evaporation-induced flow may trigger colloidal glass's crystallization. We infer the subsequent propagation of crystal growth front to be promoted by the reduction of glass mechanical stability due to the sedimentation-induced density decrease. However, when the density at the crystal growth front reaches a threshold above which mechanical instability cannot be induced, the front should stop proceeding. Since this explanation is speculative, its validity needs to be checked in the future.

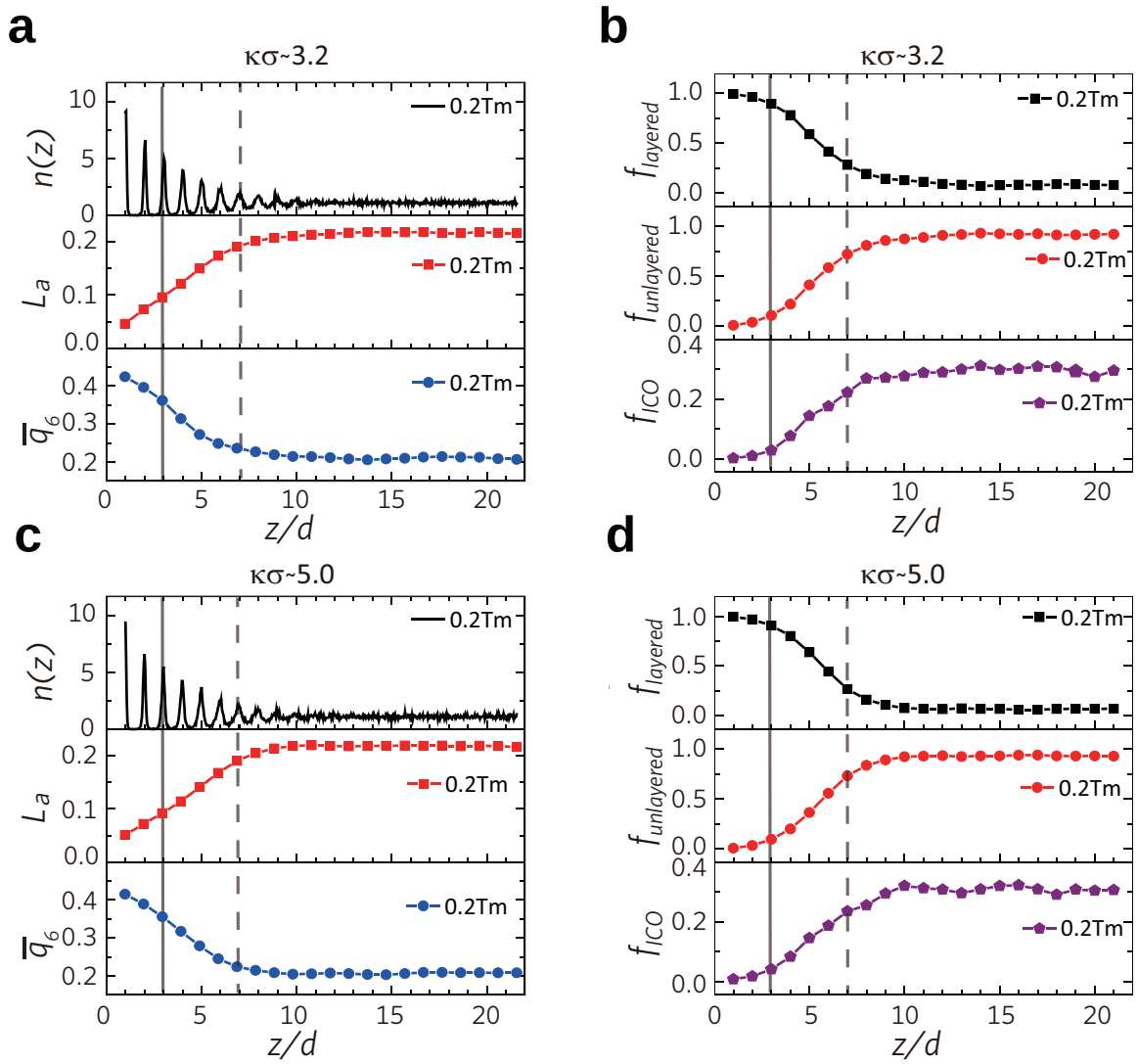

FIG. S1: **The interface profile of fast crystal growth at $T = 0.2T_{\rm m}$ for $\kappa\sigma \sim 3.2$ and $\kappa\sigma \sim 5.0$. a,** Interface profile for $\kappa\sigma \sim 3.2$ illustrated by the z/d-dependences of the particle number density $n(z)$ (top), $L_a(z)$ (middle), and $\overline{q}_6(z)$ (bottom). **b,** Interface profile illustrated by the fractions of layered structures $f_{layered}$ (top), unlayered structures $f_{unlayered}$ (middle), and icosahedron (ico)-like structures f_{ico} (bottom) in each layer. **c, d,** Interface profile for $\kappa\sigma \sim 5.0$ illustrated by the z/d-dependences of the same quantities as in **a** and **b**, respectively. The similar rough and thick interface provides a "buffer zone" that disintegrates the abundant ico-like structures ($\sim$ 30 % in the unlayered liquid). The meaning of the grey vertical solid and dashed lines are the same as those in Fig. 1e and f.

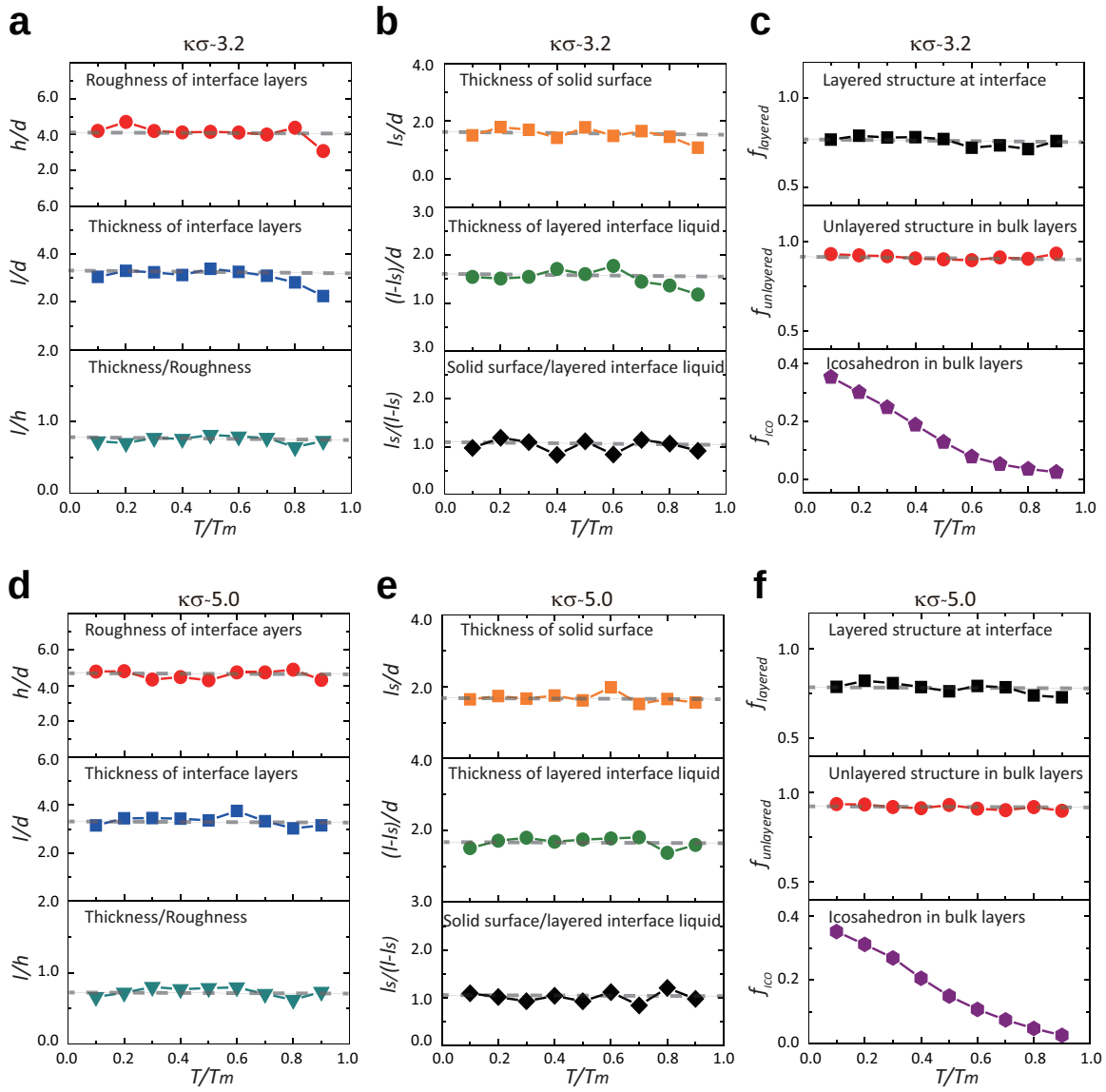

FIG. S2: **The T-dependence of interface characteristics for $\kappa\sigma \sim 3.2$ and $\kappa\sigma \sim 5.0$. a,** The T-dependence of the roughness h, thickness l and l/h for $\kappa\sigma \sim 3.2$. At each panel, the grey line indicates the average value. **b,** The T-dependence of the solid surface thickness l_s, interface liquid thickness $l - l_s$ and $l_s/(l - l_s)$ for $\kappa\sigma \sim 3.2$. **c,** The T-dependence of $f_{layered}$ (the fraction of layered particles at interface), $f_{unlayered}$ (the fraction of unlayered particles at interface) and f_{ico} (the fraction of icosahedron (ico)-like particles in bulk layers) for $\kappa\sigma \sim 3.2$. **d-f,** The same as **a-c** for $\kappa\sigma \sim 5.0$. The basic characteristics of the roughess, thickness, and and layered nature of the interface is little affected by the increasing amount of ico-like structures in the bulk due to deeper supercooling.

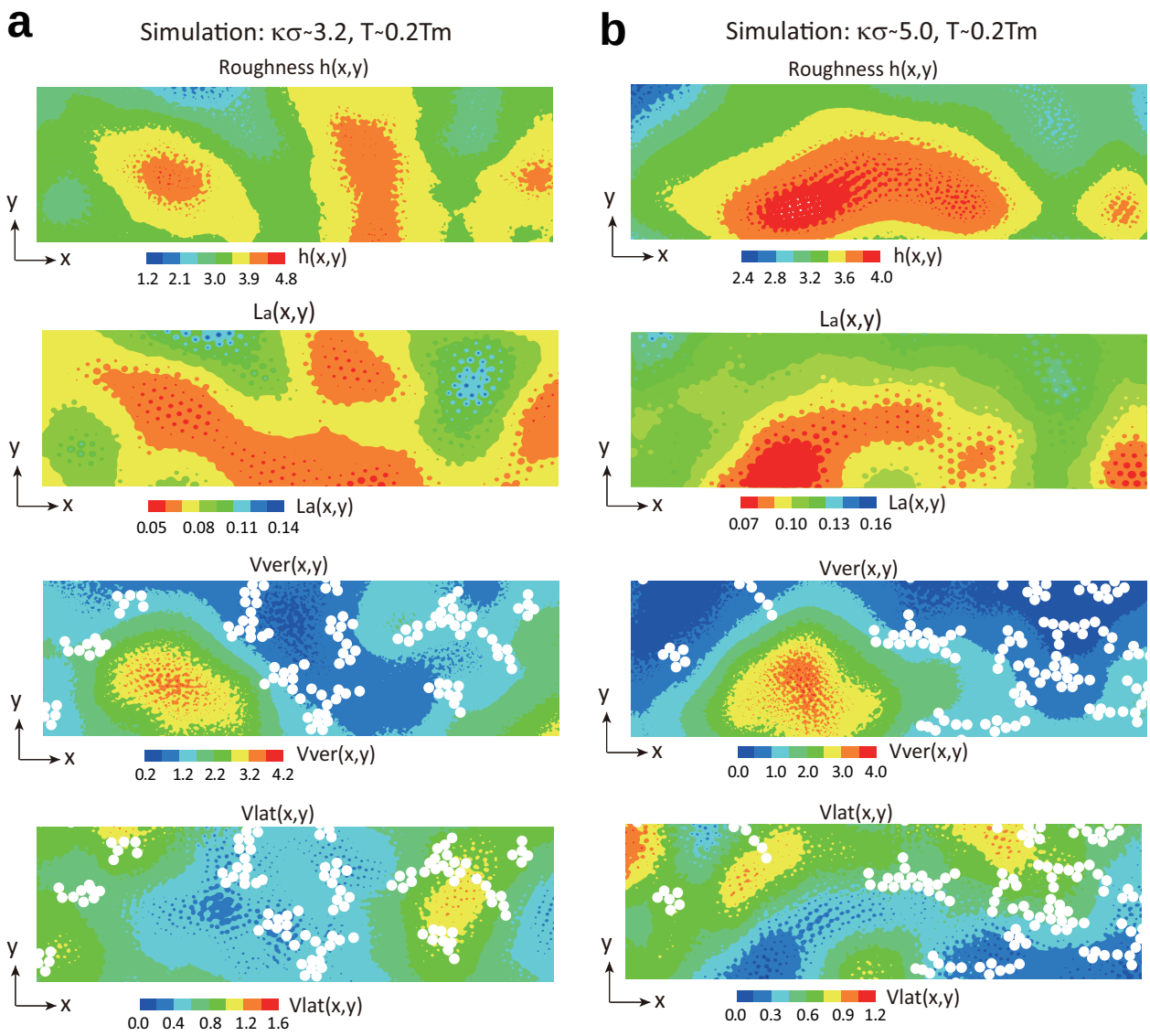

FIG. S3: **The low-T island-growth mode of crystals for rough and thick interfaces for $\kappa\sigma \sim 3.2$ and $\kappa\sigma \sim 5.0$. a,** Contour plots of the height of the crystal front $h(x, y)$, $L_a(x, y)$, $v_{ver}(x, y)$, and $v_{lat}(x, y)$ from top to bottom, respectively, for $\kappa\sigma \sim 3.2$ at $T \sim 0.2T_{\rm m}$. **b,** The same as **a** for $\kappa\sigma \sim 5.0$ at $T \sim 0.2T_{\rm m}$. We can see the vertical growth mode generating new islands as well as the lateral growth mode around the island. The abundant icosahedron-like particles (white spheres) at the interface is predominantly eliminated by the lateral growth of crystals in **a** and **b**.

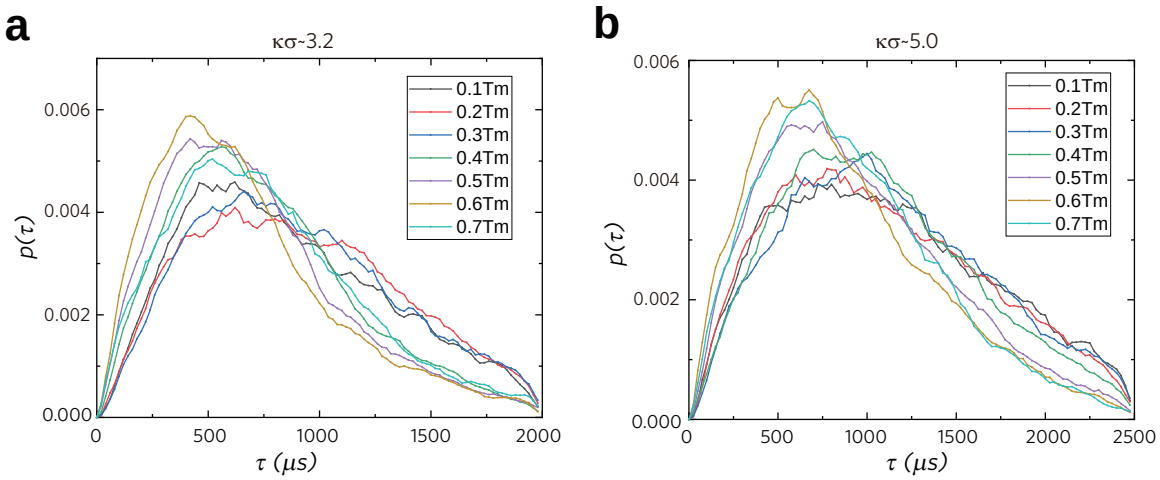

FIG. S4: **Probability distribution of τ, $p(\tau)$, for $\kappa\sigma \sim 3.2$ and $\kappa\sigma \sim 5.0$ at various T.** We can see the T-insensitivity of $p(\tau)$ for both $\kappa\sigma \sim 3.2$ (**a**) and $\kappa\sigma \sim 5.0$ (**b**).

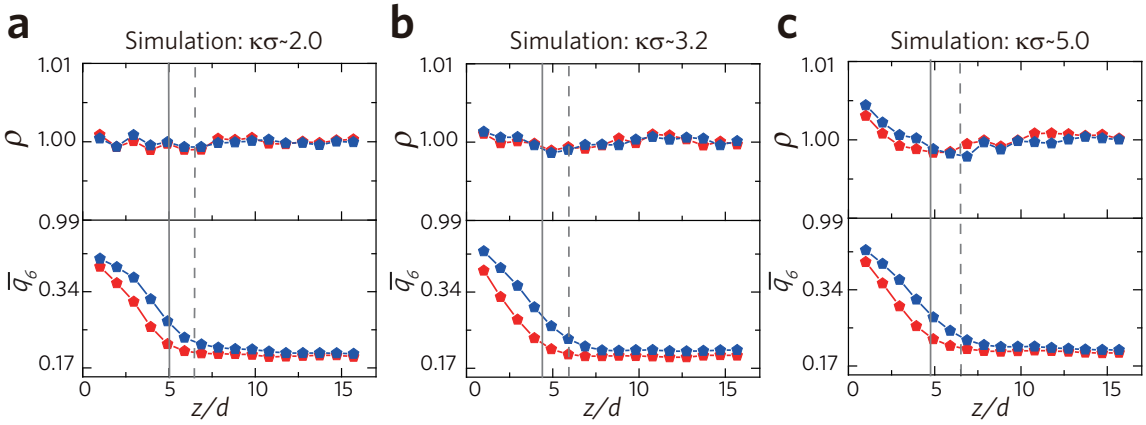

FIG. S5: **The z/d-dependences of the density and structural order during crystal growth at $T = 0.1T_{\rm m}$ for $\kappa\sigma \sim 2.0$, $\kappa\sigma \sim 3.2$ and $\kappa\sigma \sim 5.0$ (simulations). a,** The z/d-dependences of the normalized density $\rho(z)$ ($= \rho_{local}(z)/\rho_0$) (top panel) and structural order $\overline{q}_6(z)$ (bottom) for $\kappa\sigma \sim 2.0$. Here, $\rho_{local}(z)$ is the number of particles in each layer at z divided by the total Voronoi cell volume of particles in the same layer and $\rho_0 = N/V$. The red and blue curves represent the profiles at different times. The vertical solid and dashed lines represent the average interface z-positions (the interface front adjacent to the liquid) for the red and blue curves, respectively. **b, c,** The same as **a** for $\kappa\sigma \sim 3.2$ and $\kappa\sigma \sim 5.0$. We can see that the structural ordering is accompanied by little density variation (< 1 %) across the interface for all $\kappa\sigma$. We can notice the slight increase of the crystal-liquid density mismatch with the increase of $\kappa\sigma$.

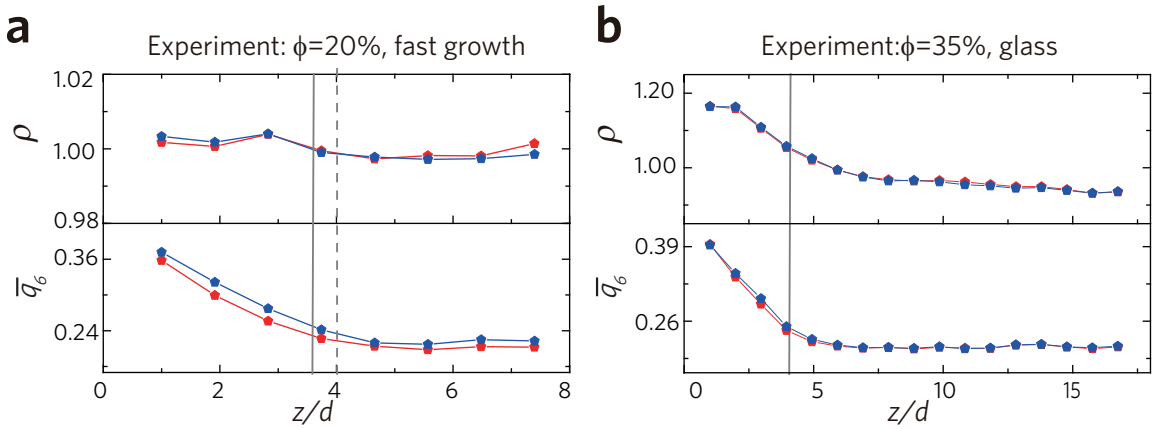

FIG. S6: **Comparison of the z/d-dependences of the density and structural order between fast-crystal-growth interface in a deeply supercooled liquid ($\phi \sim 20$ %) and crystal-glass interface ($\phi \sim 35$ %) in experiments. a,** The z/d-dependences of the normalized density, ρ ($\rho = \rho_{local}(z)/\rho_0$, top), and $\overline{q}_6(z)$ (bottom) at $\kappa\sigma \sim 2.0$ for a typical deeply-supercooled sample (the particle volume fraction $\phi \sim 20$ %), which exhibits the fast crystal growth induced by the flat wall. The red and blue curves represent the profiles at different times. The vertical solid and dashed lines represent the average interface z-position for the red and blue curves, respectively. **b,** The same as **a** for a typical glass sample with a few layers of crystal induced by the flat wall ($\phi \sim 35$ %). We can see that the structural ordering is accompanied by little density variation (< 1 %) across the interface in **a**, similarly to the corresponding simulations, whereas there is a considerable crystal-glass density mismatch (~ 20 %) in **b**.

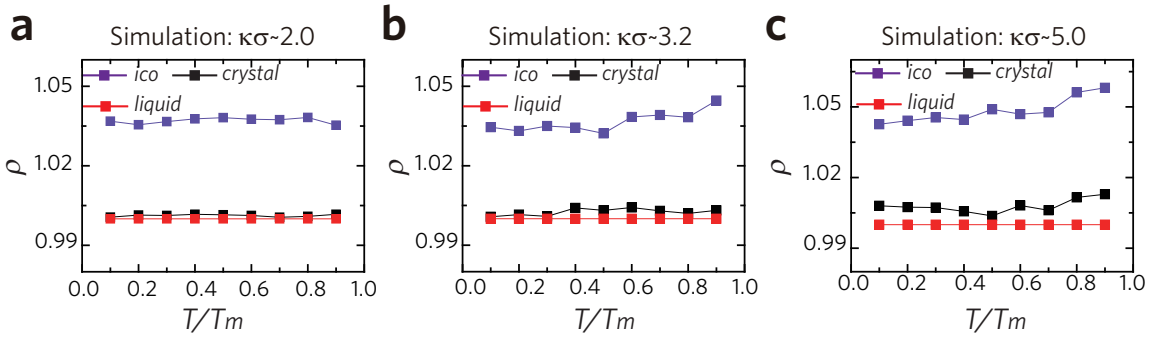

FIG. S7: **Weak T-dependence of the density profile for $\kappa\sigma \sim 2.0$, $\kappa\sigma \sim 3.2$, and $\kappa\sigma \sim 5.0$ (simulations) during fast crystal growth (when the solid fraction ~ 25 %). a,** The T-dependences of the densities of crystal ($\rho_{\rm crys}$), supercooled liquid ($\rho_{\rm liq}$) and nearly-perfect icosahedron ($\rho_{\rm ico}$) structures normalized by ρ_0 ($\rho_0 = N/V$) for $\kappa\sigma \sim 2.0$. **b, c,** The same as **a** for $\kappa\sigma \sim 3.2$ and $\kappa\sigma \sim 5.0$. The T-dependence of the crystal density is very weak for all three cases. We can see that the ico-like structures has the largest local density among the three types of structures. We can also notice the slight increase of the crystal-liquid density mismatch with an increase in $\kappa\sigma$.

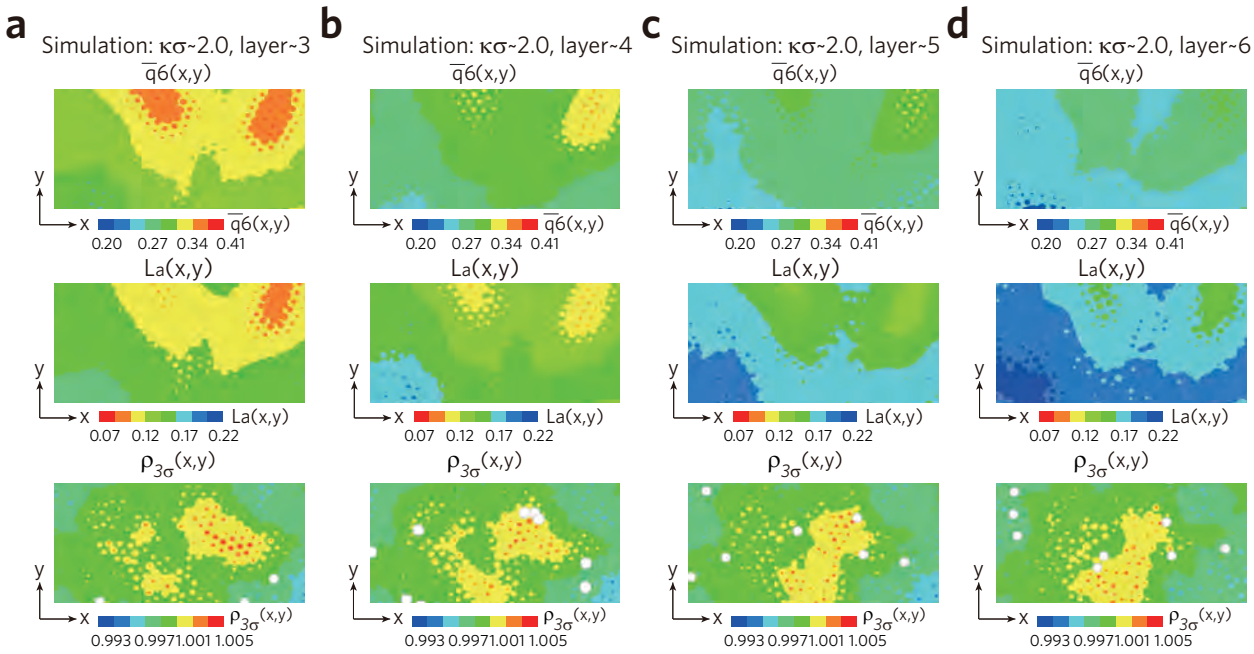

FIG. S8: **The z/d-dependence of the structural features in the x-y plane in the interface region for $\kappa\sigma \sim 2.0$ at $T = 0.1T_{\rm m}$ (simulations). a,** Contour plots of $\overline{q}_6(x, y)$ (top), $L_a(x, y)$ (middle), $\rho_{3\sigma}(x, y)$ (bottom, ρ_{local} coarse-grained with 3σ) at $z/d = 3$. The ico-like particles are represented by white spheres. **b-d,** The same as **a** for z/d=4, 5, and 6, respectively. We can see that the structural ordering is accompanied by little density change across the interface. At each z, the amplitude of spatial fluctuation of $\rho_{3\sigma}(x, y)$ is more significant than the crystal-liquid density mismatch, indicating little density effect on structural ordering.

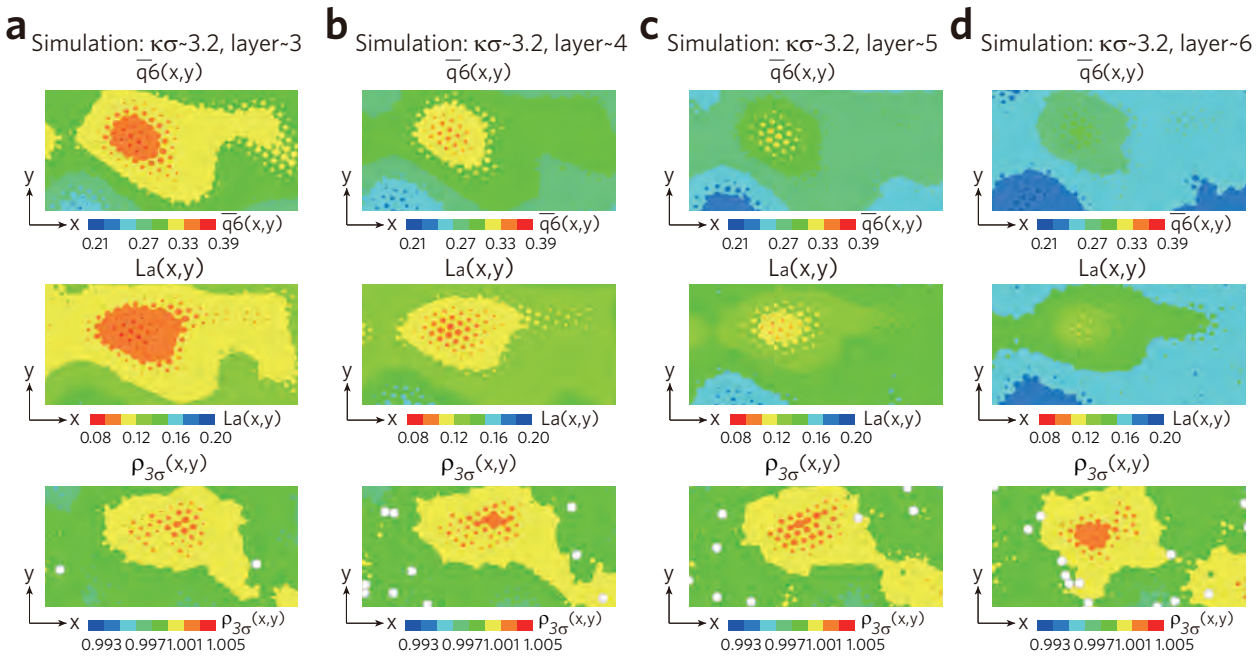

FIG. S9: **The z/d-dependence of the structural features in the x-y plane in the interface region for $\kappa\sigma \sim 3.2$ at $T = 0.1T_{\rm m}$ (simulations). a,** Contour plots of $\overline{q}_6(x, y)$ (top), $L_a(x, y)$ (middle), and $\rho_{3\sigma}(x, y)$ (bottom, ρ_{local} coarse-grained with 3σ) at $z/d = 3$. The ico-like particles are represented by white spheres. **b-d,** The same as **a** for z/d=4, 5, and 6, respectively. We can see that the structural ordering is accompanied by little density change across the interface. At each z, the amplitude of spatial fluctuation of $\rho_{3\sigma}(x, y)$ is more significant than the crystal-liquid density mismatch, indicating little density effect on structural ordering. Note that a dense, disordered region appears at the lower-right corner of panels c and d.

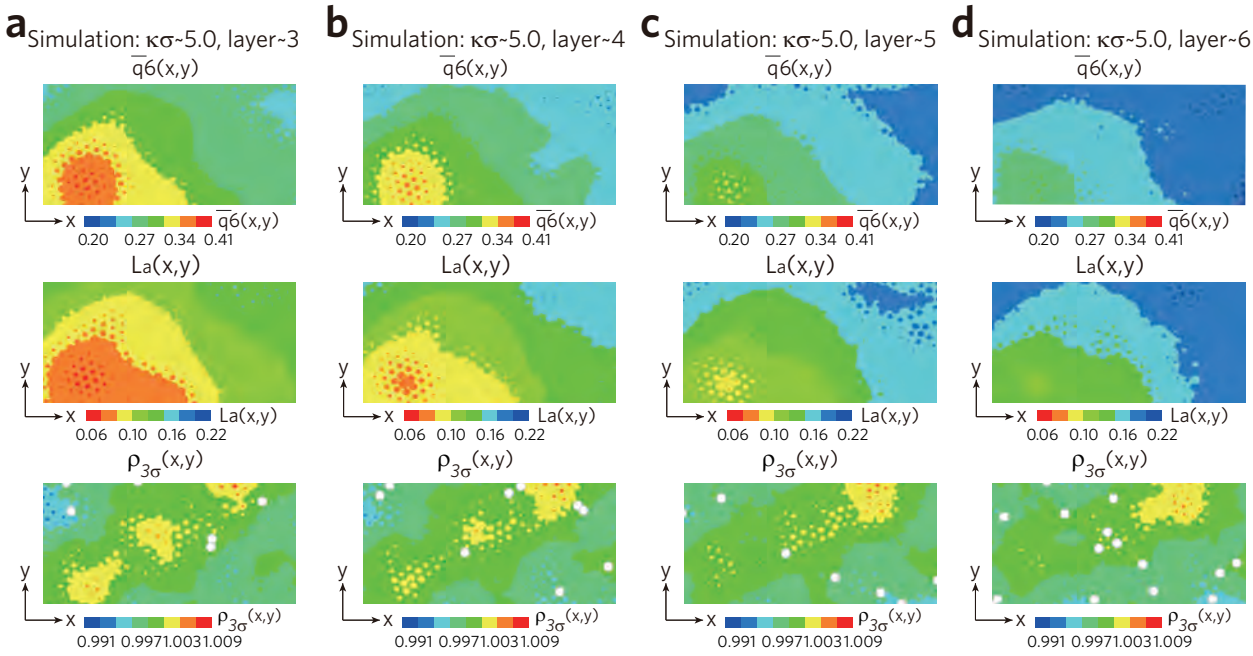

FIG. S10: **The z/d-dependence of the structural features in the x-y plane in the interface region for $\kappa\sigma \sim 5.0$ at $T = 0.1T_{\rm m}$ (simulations). a,** Contour plots of $\overline{q}_6(x, y)$ (top), $L_a(x, y)$ (middle), and $\rho_{3\sigma}(x, y)$ (bottom, ρ_{local} coarse-grained with 3σ) at $z/d = 3$. The ico-like particles are represented by white spheres. **b-d,** The same as **a** for z/d=4, 5, and 6, respectively. We can see that the structural ordering is accompanied by little density change across the interface. At each z, the amplitude of spatial fluctuation of $\rho_{3\sigma}(x, y)$ is more significant than the crystal-liquid density mismatch, indicating little density effect on structural ordering. Note that a dense, disordered region appears at the upper-right corner of panels b, c, and d.

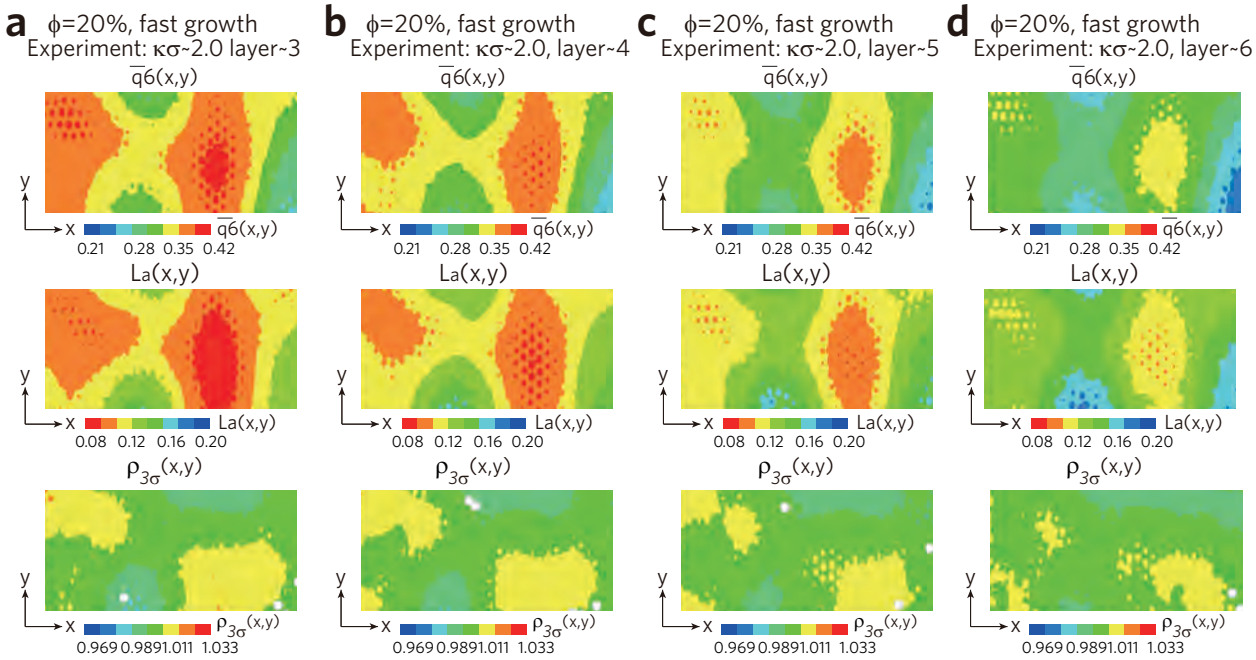

FIG. S11: **The z/d-dependence of the structural features in the x-y plane in the interface region for $\kappa\sigma \sim 2.0$ at $T = 0.5T_{\rm m}$ (experiments). a,** Contour plots of $\overline{q}_6(x, y)$ (top), $L_a(x, y)$ (middle), and $\rho_{3\sigma}(x, y)$ (bottom, ρ_{local} coarse-grained with 3σ) at $z/d = 3$. The ico-like particles are represented by white spheres. **b-d,** The same as **a** for z/d=4, 5, and 6, respectively. We can see that the structural ordering is accompanied by little density change across the interface. At each z, the amplitude of spatial fluctuation of $\rho_{3\sigma}(x, y)$ is more significant than the crystal-liquid density mismatch, indicating little density effect on structural ordering. Note that a dense, disordered region appears at the bottom-right corner of each panel in **d**.

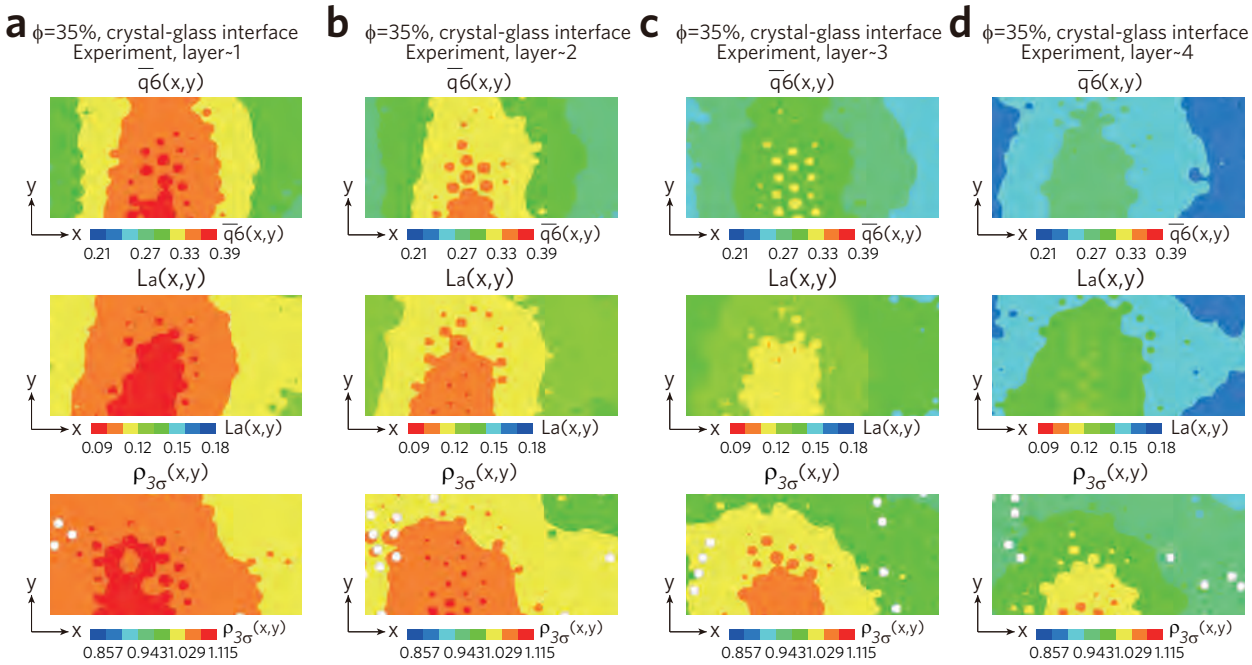

FIG. S12: **The z/d-dependence of the structural features in the x-y plane at $\phi \sim 35$ % (experiments). a,** Contour plots of $\overline{q}_6(x,y)$ (top), $L_a(x,y)$ (middle), and $\rho_{3\sigma}(x,y)$ (bottom, ρ_{local} coarse-grained with 3σ) at $z/d = 1$. The ico-like particles are represented by white spheres. **b-d,** The same as **a** for z/d=2, 3, and 4, respectively. We can see that the order growth is accompanied by large density change across the interface. The crystal-glass density mismatch is much larger than the amplitude of spatial fluctuation of $\rho_{3\sigma}(x,y)$ in the disordered region. At each z, we find strong correlation between the densest and highly ordered regions.

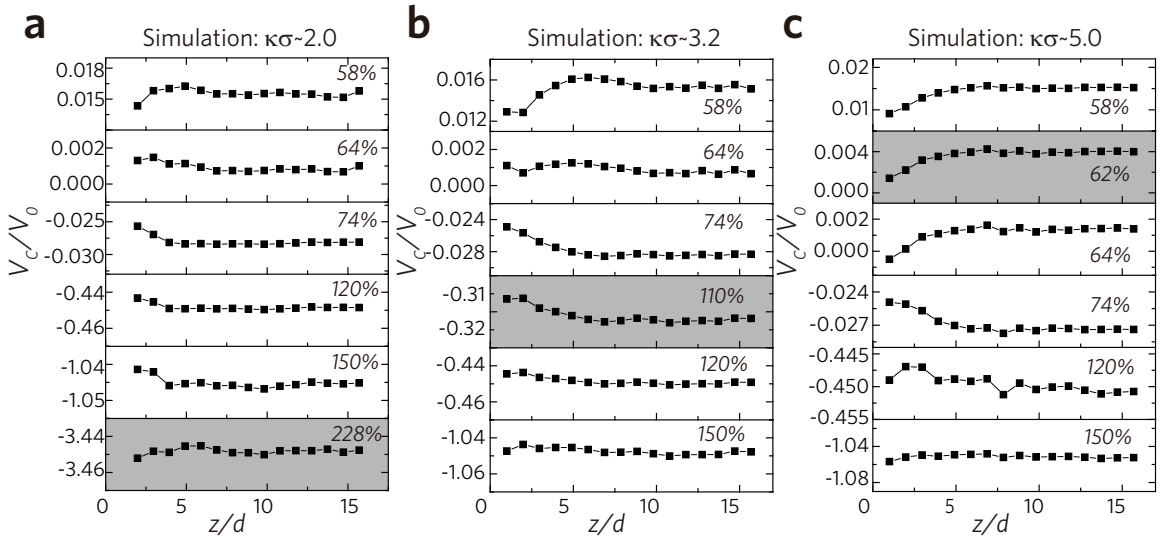

FIG. S13: **The z/d-dependence of the free volume or overlapped volume, V_c, at $T = 0.1T_{\rm m}$ for $\kappa\sigma \sim 2.0$, $\kappa\sigma \sim 3.2$ and $\kappa\sigma \sim 5.0$ (simulations).** We use a reference radius r_c, which is defined as the effective radius of each particle in the configuration, to calculate the r_c-dependent free or overlapped volume, V_c. Here, $V_c(i) = \Sigma_{j=1}^{Nb}(d_{ij} - 2r_c)^3$, where Nb is the neighbour number of particle i (i.e, the number of particles around particle i within the first minimum distance of the radial distribution function), and d_{ij} is the bond length between particle i and neighbour particle j. V_c is then divided by the average Voronoi cell volume V_0. For the free-volume dominating regime, $V_c/V_0 > 0$, whereas for the overlapped-volume dominating, $V_c/V_0 < 0$. We select the values of r_c as those corresponding to $\phi(r_c) \sim 0.58$, 0.64, 0.74, 1.20 and 1.50 ($\phi(r_c) = \frac{4\pi r_c^3}{3V_0}$). The r_c value at which the pair potential $u(r) = k_B T_{\rm m}$ is shown by the grey-shaded panel. **a,** The z/d-dependence of V_c/V_0 for various r_c at $\kappa\sigma \sim 2.0$. We can see that the ordering has very little effect on the free volume for $\phi(r_c) \leq 0.64$ whereas the ordering slightly reduces the overlapped volume (about 0.5 %) for $0.74 \leq \phi(r_c) \leq 1.2$. Note that $u(r) = k_B T_{\rm m}$ corresponds to a volume fraction of 2.28. In this case, the overlapped volume effect estimated from the the short r_c (within the first neighbour shell) is very weak, suggesting that preordering mainly drives the crystal growth. **b, c,** The z/d-dependence of V_c/V_0 for various r_c at $\kappa\sigma \sim 3.2$ and $\kappa\sigma \sim 5.0$, respectively. We can see that the structural ordering in these cases also only slightly reduces the overlapped volume for $0.74 \leq \phi(r_c) \leq 1.2$ (about 0.5 %). The results also suggest the prevealing effect of preordering on crystal growth.

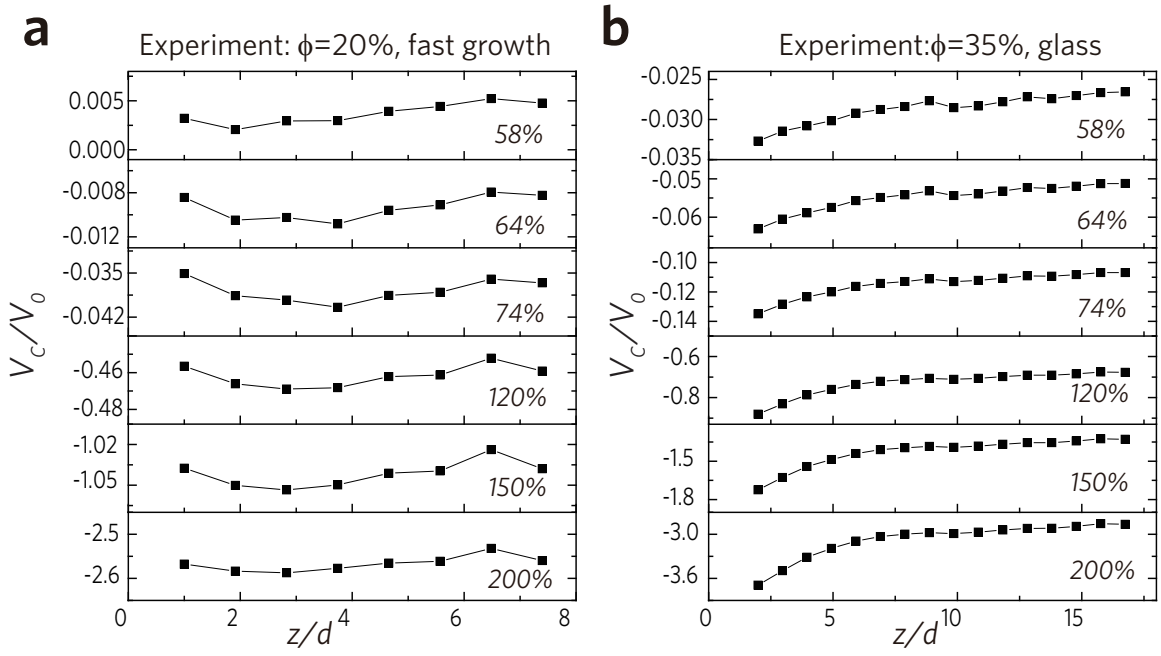

FIG. S14: **Comparison of the z/d-dependence of the free volume or overlapped volume for fast-crystal-growth interface in a deeply supercooled liquid ($\phi \sim 20$ %) and crystal-glass interface ($\phi \sim 35$ %) in experiments.** The analysis employed is the same as in Fig. S13. We select the values of r_c as those corresponding to $\phi(r_c) \sim 0.58$, 0.64, 0.74, 1.20, 1.50 and 2.00 ($\phi(r_c) = \frac{4\pi r_c^3}{3V_0}$). **a,** The z/d-dependence of V_c/V_0 for various r_c at $\phi \sim 20$ %. We can see that the structural ordering has little effect on both the increase of the free volume at $\phi(r_c) \sim 0.58$ and 0.64 and the reduction of the overlapped volume for $\phi(r_c) \leq 2.0$ (<1 %). In these cases, thus, the preordering should be mainly responsible for fast crystal growth as in simulations. **b,** The z/d-dependence of V_c/V_0 for crystal-glass interface ($\phi \sim 35$ %) at various r_c. We can see that the structural ordering tends to increase the overlapped volume for $0.64 \leq \phi(r_c) \leq 2.0$, which is caused by the large crystal-glass density mismatch. This result suggests that the large crystal-glass density mismatch blocks the crystallization of the preordered interface.

SUPPLEMENTARY REFERENCES

[1] Pusey, P. N. & Van Megen, W. Phase behaviour of concentrated suspensions of nearly hard colloidal spheres. *Nature* **320**, 340–342 (1986).

[2] Van Megen, W. & Underwood, S. Change in crystallization mechanism at the glass transition of colloidal spheres. *Nature* **362**, 616–618 (1993).

[3] Pusey, P. *et al.* Hard spheres: crystallization and glass formation. *Philos. Trans. R. Soc. A: Math. Phys. Eng. Sci.* **367**, 4993–5011 (2009).